Journal of Molecular Graphics and Modelling 61 (2015) 107–114

Contents lists available at ScienceDirect

Journal of Molecular Graphics and Modelling

journal homepage: www.elsevier.com/locate/JMGM

Geometric rules of channel gating inferred from computational models of the P2X receptor transmembrane domain

Guo-Hua Li

School of Life Sciences, Changchun Normal University, Changchun 130032, China

ARTICLE INFO

Article history:
Received 23 March 2015
Received in revised form 1 June 2015
Accepted 29 June 2015
Available online 9 July 2015

Keywords:
P2X
Ion channel
Molecular dynamics
Transmembrane helix
Channel gating
Helical packing

ABSTRACT

The P2X receptors are trimeric ATP-gated ion channels and mediate chemical communication between eukaryotic cells. Each P2X subunit contains two transmembrane helices, M1 and M2, and the M2 helix packs around an ion conduction pore. Here, I have reconstructed the three-dimensional models of the zebrafish P2X4 transmembrane domain using spatial restraints on helical packing. The models are stable in lipid bilayers during molecular dynamics simulation and adopt different conformations depending on bilayer hydrophobic thickness. Comparison of these conformations shows that the pore-lining residues L340, A344 and A347 each have multiple packing sites that define the pore configurations. Shift of L340 packing between different sites alters the side-chain orientation that occludes the pore or removes this occlusion. L340, A344 and A347 also gate the pore by expansion–contraction mechanism based on their packing patterns. Finally, pore expansions at the L340 and A344 levels are mutually exclusive, so the P2X gating may involve sequential pore opening at L340 and A344 levels to allow ion conduction. In summary, the current study shows that the computational assembly of the helical membrane protein is not only possible, but also necessary to provide insights into the mechanisms of channel gating.

1. Introduction

An ion channel is a transmembrane protein that allows ions to move across the plasma and intracellular membranes. The protein is typically composed of several subunits organized around a central ion conduction pore. The pore is lined dominantly by α-helices, and usually gated by particular stimuli such as ligand-binding. The ATP-gated ion channel, namely the P2X receptor (P2XR), is a trimeric protein with two transmembrane helices (M1 and M2) in each subunit. The M2 helix packs around the ion conduction pathway, with the amino acid residues L340, A344 and A347 lining the pore lumen [13,5].

The interhelical packing is a key element in defining the tertiary and quaternary structures of helical membrane proteins and has been simplified to a four-residue tetrahedral packing unit where a knob residue packs into a three-residue socket [11]. Currently I examined the possibility of computational assembly of the P2X transmembrane domain (TMD) based on spatial arrangement of tightly packed residues and gaining insights into channel gating mechanisms from such computational models. The assembly follows the two-stage protein folding scheme [21]. First, geometrically regular α-helices for M1 and M2 are relaxed independently in a lipid bilayer by molecular dynamics (MD) simulation. Second, these helices are assembled into a tertiary TMD (tTMD) and then a quaternary TMD (qTMD) based on spatial restraints on interface residues.

The intrasubunit packing of the zebrafish (zf) P2X4.1 occurs between the knob residues V42 and V46 on M1 and their target residues on M2. The packing patterns differ for the apo (PDB codes: 4DW0, 3I5D and 3H9V) and the ATP-bound (PDB code: 4DW1) forms. In the apo-form models such as 4DW0, 3I5D and 3H9 V, V42 packs into a pocket formed by G345, L348, L349 and V352, while V46 packs into a pocket formed by N341, I342 and G345. In the 4DW1 model, both V42 and V46 shift by a small distance toward the C-terminus so that V42 packs into a pocket formed by L348, L349 and V352, and V46 sits on G345. This information was used to guide the assembly of the P2X-tTMD. In the 4DW0, 3I5D and 3H9 V models, the intersubunit packing occurs between neighboring M2 helices. The L340 and L346 side-chains on one M2 helix pack into their pockets on the clockwise neighboring (referred to as downstream) M2 helix. The pocket for L340 is formed by L340, N341 and A344 (denoted as LN:A), and the pocket for L346 is formed by A347, L348 and L351 (denoted as AL:L). This information was used to guide the assembly of the P2X-qTMD. The intersubunit packing is absent in the 4DW1 model.

E-mail address: licharles35@gmail.com

http://dx.doi.org/10.1016/j.jmgm.2015.06.015
1093-3263/

Functional P2X receptors are organized as trimers and structural models at the quaternary level are expected to provide insights into the mechanisms of channel gating. Therefore, the qTMD models were more fully investigated using MD simulation in different lipid bilayers to enhance the conformational sampling. The lipids used in this study are 1,2-dilauroyl-*sn*-glycero-3-phosphocholine (DLPC), 1-palmitoyl-2-oleoyl-*sn*-glycero-3-phosphocholine (POPC), and 1-stearoyl-2-oleoyl-*sn*-glycero-3-phosphocholine (SOPC). They differ in unsaturation and length of the acyl chains, thus produce bilayers of different hydrophobic thickness [17]. The current computational results suggest that changes in intersubunit packing pattern for the residues L340, A344 and A347 play an important role in channel gating in the P2X receptors and such changes are driven by hydrophobic matching between lipids and transmembrane helices.

2. Methods

2.1. Computational structure assembly

The process of computational assembly of the zfP2X4 TMD is comprised of 3 steps: (1) secondary structure refinement, (2) tertiary structure assembly, and (3) quaternary structure assembly. For secondary structure refinement, geometrically ideal α-helices, referred to as S1 and S2, were built with backbone dihedral angles (ϕ, ψ) around (-58°, -47°). S1 covers 30 residues of zfP2X4 from S28 to Y57, and S2 covers 29 residues from F333 to L361. Each helix was vertically inserted into a POPC bilayer, and subjected to 10-ns MD relaxation. The relaxed structures are used as the building blocks for assembly of higher-level structures by structural alignment or residue packing.

Here the term residue packing refers to a process by which the tertiary or quaternary structure is assembled according to the spatial arrangement of tightly packed residues. When a template is available, the simplest way to pack the knob and socket residues of the modeled structure is to align them to their counterparts of the template. For assembly of P2X-tTMD, the relaxed S2 is superimposed on a template (4DW1 or 4DW0) in a way that the Cα-atoms of the pocket residues N341, I342, G345, L348, L349 and V352 are aligned, and the relaxed S1 is superimposed on the template in a way that the Cα-atoms of the knob residues V42 and V46, as well as A44 were aligned. The use of A44 is due to the fact that at least three positions are required to uniquely define the coordinates of the S1 helix. The aligned S1 and S2 were combined to form a tertiary model. The 4DW0- and 4DW1-based tertiary models are referred to as P0-tTMD and P1-tTMD, respectively. Each model was inserted in a bilayer composed of 166 POPC molecules and relaxed by 5-ns MD run. The MD simulation system contains 10,885 water molecules. After relaxation, a loop was built to connect S1 and S2.

For assembly of the P2X-qTMD, a dimer is assembled by packing L340 and L346 on a tTMD (denoted as subunit A) to their pockets on the downstream tTMD (denoted as subunit C). Then a trimer was assembled by packing L340 and L346 of subunit C to their pockets on a third tTMD (denoted as subunit B). Since the refined P0- and P1-tTMDs are highly similar to each other (see the Results and Discussion Section), only refined P1-tTMD was used for quaternary assembly and the resultant trimeric complex is referred to as P0-qTMD. For comparison, another qTMD model was built by merging copies of P1-tTMD aligned to different chains of 4DW0 model (referred to as A0-qTMD).

2.2. Molecular dynamics

Protein models were embedded [25] in lipid bilayers solvated by TIP3P water molecules [12] and neutralized with sodium and chloride ions at a 0.13 M concentration. The *Z*-axis of the coordinate system coincides with the bilayer normal and points toward the extracellular side of the protein model. The system energy was minimized by 1000 cycles of the steepest descent algorithm. The process of MD relaxation was divided into two phases: restrained MD and 60-ns unrestrained MD. The restrained MD simulation was composed of 100 short (5-ps) runs and each run was carried out with harmonic position restraint (force constant 100 kJ/mol/nm^2) of Cα to the starting conformation of each run. This allows gradual adjustment of local structures in lipid environment. For MD simulation of the 4DW0-qTMD, hydrogen atoms were added and incomplete residues were fixed with the homology modeling software Modeller (version 9.13, [23]).

MD simulation was performed with GROMACS 5.0.2 and 5.0.4 based on CHARMM36 forcefield [3,15,9]. The LINCS algorithm [6] was used to constrain all bond lengths so that a 2-fs integration time step could be used. The protein, lipid and ion-water were coupled separately to a v-rescale thermostat at 310 K with a coupling constant of 1-ps. A constant pressure of 1 bar was applied independently in the *xy*-plane (the lipid-plane) and the z directions with a coupling constant of 1-ps. Periodic boundary conditions were applied and Lennard–Jones interactions were truncated at 1.2 nm. Electrostatic interactions were calculated using the particle mesh Ewald method [4] with a real space cutoff of >1.2 nm on an approximately 0.16-nm grid with fourth-order spline. The MD simulation was carried out on GPU-accelerated computers (an Intel Core i7-3770CPU plus a GTX 780 GPU, and an AMD Phenom II X6 six-core 1075T CPU plus a GTX 680 GPU).

2.3. Geometric properties of helical organization

The properties of the quaternary TMD are described in terms of helix tilts, helix crossing angles, and the pore shapes. To define the tilt and crossing angles, two lines (denoted L1 and L2) were defined for S1 and S2. L1 is defined by the projections of V42 and V46 Cα atoms along the helix axis, and L2 is defined by the projections of G345 and V352 Cα atoms along the helix axis. The tilt angle of S1 is defined as the angle between *Z*-axis and L1, and the tilt angle of S2 is made between *Z*-axis and L2. The crossing angle in a tertiary TMD structure is defined as the angle between L1 and L2.

The pore geometry was calculated by the program HOLLOW [8] with grid-spacing of 0.15 Å. To describe pore expansion or constriction, three triangles are defined: the L340 triangle, the A344 triangle and the A347 triangle, each is defined by the corresponding Cα atoms as the vertexes, and the sides of the triangles are defined by the distances between the Cα atoms (DCα) at each interface. These triangles are referred to as the gating triangles.

2.4. Residue contact criterion, helix packing and residues at helix crossing points

Two residues within different transmembrane helices are considered in contact if the minimal distance between atoms is less than 2.9 Å. A residue is defined as a knob residue if it is in contact with at least two residues and the knob residue and the residues in contact form a packing unit. The tightness of packing is defined by a packing distance (PD) which is the average of two minimum distances. In most cases, the knob residue packs into a three-residue pocket at relative positions *i*, *i*+1 and *i*+4 or *i*, *i*+3 and *i*+4. For example, the residues L340, N341 and A344 form a pocket for the side-chain of L340 of the counter-clockwise neighboring (referred to as upstream) M2 helix, and these residues are denoted as LN:A, where the colon indicates sequence separation of 2.

For a residue *R* and a helix *j*, where *R* is on a different helix, the distance between residue *R* and helix *j* is defined to be the minimal distance between the Cα atom of the residue and the axis of helix *j*.

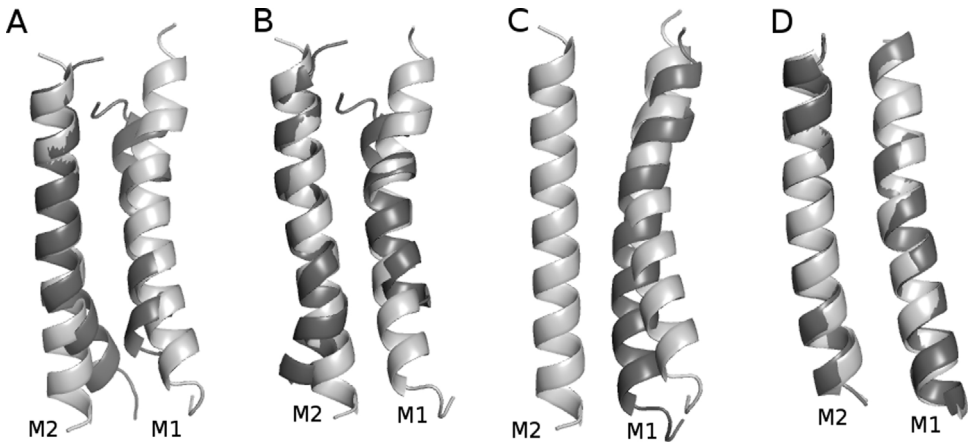

Fig. 1. Crystal and computational structures of the tertiary P2X transmembrane domain. (A) Superimposition of the 4DW0 model (dark grey) and the P0-tTMD (light grey). (B) Superimposition of the 4DW1 model (dark grey) and the P1-tTMD (light grey). (C) Comparison of the P0-tTMD (dark grey) and P1-tTMD (light grey) models, with the M2 helices aligned. (D) Comparison of P0-tTMD (dark grey) and P1-tTMD (light grey) after 10-ns MD simulation, with the M2 helices aligned.

For two packed helices *i* and *j*, the residue on helix *i* with minimal residue to helix distance is said to be at the crossing point. The residue at the crossing point on helix *j* is similarly determined.

3. Results and discussion

3.1. Assembly of the tertiary TMD models

After refinement in the POPC bilayer by 10-ns MD simulation, the Cα-RMSDs of S1 are 3.35 Å from 4DW0 and 3.09 Å from 4DW1, and the S2 helix deviates by less than 3 Å from 4DW0 (2.60 Å) and 4DW1 (1.87 Å). The tilt angles averaged over the last 5-ns MD run are 7.20 and 8.30° for S1 and S2, respectively. S1 and S2 are then packed into two models: P0-tTMD based on 4DW0 and P1-tTMD based on 4DW1 (Fig. 1). The helix crossing angles of P0-tTMD and P1-tTMD are 28.81 and 18.76°, respectively. For comparison, the helix crossing angles of 4DW0 and 4DW1 are 34.08 and 15.85°, respectively. The Cα-RMSDs of P0- and P1-tTMDs are 3.95 and 3.28 Å from 4DW0 and 4DW1, respectively, and reduce to 3.34 and 2.69 Å after 5-ns MD refinement. In spite of conformational differences in the starting structures, the refined P0- and P1-tTMDs are highly similar to each other, deviating by a Cα-RMSD value of 0.52 Å.

3.2. The packing patterns of L340, A344 and A347 in the quaternary TMD models

The surface of the M2 helix contains two faces for inter-subunit packing, the residues L340, N341, A344, G345, A347 and L348 (denoted as LN:AG·AL) form a face receiving knob residues L340 and G343 from an upstream M2 helix, while the residues L339, L340, G343, A344, L346 and A347 (denoted as LL:GA·LA) form a face receiving knob residues A344 and A347 from a downstream M2 helix (Fig. 2). These two faces are mostly hydrophobic and contain dynamic packing pockets. In addition to the LN:A pocket mentioned above, the residues N341, A344 and G345 (denoted as N:AG) form a pocket for the upstream L340. Sometimes the residues N341, A344, G345 and L348 (denoted as N:AG:L) are all in close contact with the upstream L340. The residues L339, L340, G343 and A344 (denoted as LL:GA) enclose a region with two small pockets for the downstream A344 (Fig. 2B): one formed by L339, L340 and G343 (denoted as LL:G), and the other by L340, G343 and A344 (denoted as L:GA). The residues G343, A344, L346 and A347 (denoted as GA·LA) enclose a region where the downstream A347 side-chain packs (Fig. 2B). In short, the M2 segment from L339 to L348 (LLNIGAGLAL), here referred to as the gating segment, is involved in packing of L340, A344 and A347 (Fig. 2C). The quater-

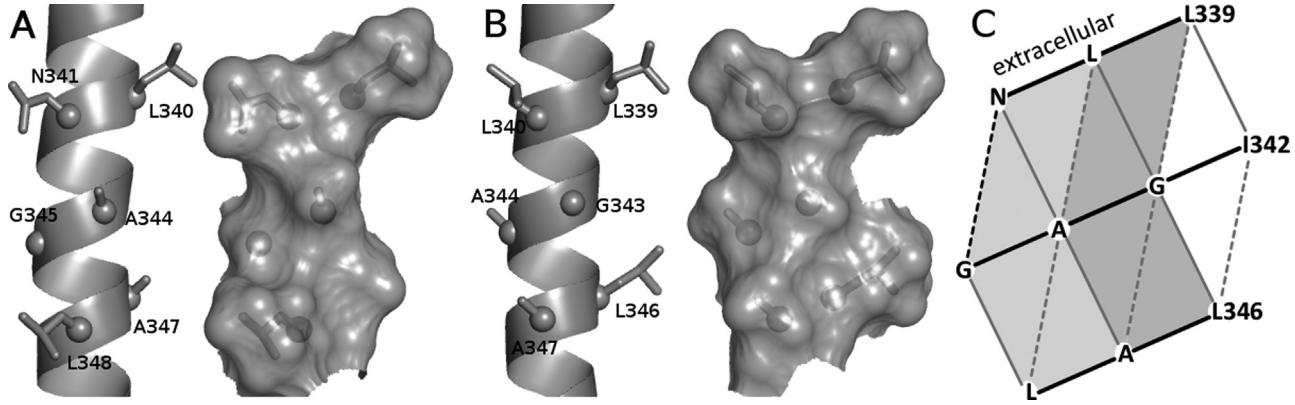

Fig. 2. Surface of the M2 helix from L339 to L348. (A) Cartoon (left) and surface (right) representations of the M2 helix showing the LN:AG·AL face for L340 and G343 packing. The structure is taken from P0-qTMD in the SOPC bilayer after 20-ns MD run. (B) The same structure is represented in cartoon (left) and surface (right) forms, showing the LL:GA·LA hydrophobic face for A344 and A347 packing. (C) The M2 helix from L339 to L348 is represented as a 2-dimensional grid, with each node as an amino acid residue. The LN:AG·AL and LL:GA·LA faces are in light and dark greys.

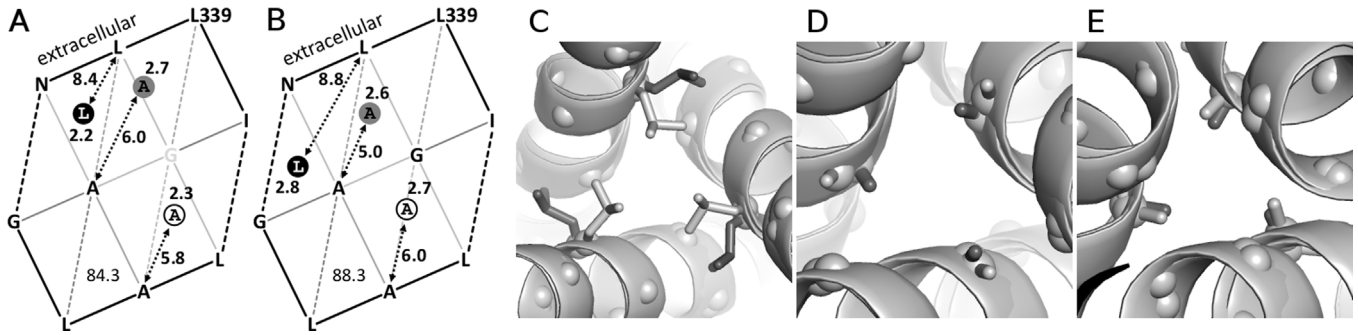

Fig. 3. Side-chain relaxation of the 4DW0 TMD by MD simulation in a DLPC bilayer. (A) and (B) are grid representations of the packing patterns of L340, A344 and A347 before and after the MD simulation, respectively. The knob residues L340, A344 and A347 are represented by circled letters, and the circle for A344 knob residue is filled. The double arrow symbols indicate the DCα distances (in Å) between a knob residue and its counterpart on the receiving helix. Numbers by the knob residues are packing distances in Å. Numbers in the A:AL regions indicate the crossing angle (in degrees) between interface M2 helices. (C), (D) and (E) Orientations of the L340, A344 and A347 side-chains before (light grey) and after (dark grey) the MD run.

nary organization of the gating segments is referred to as a gating block.

The 4DW0 model was first relaxed in a DLPC bilayer by 3-ns MD simulation with position restraints of backbone atoms (force constant 1000 kJ/mol/nm^2). The relaxed structure deviates from the starting structure by a Cα-RMSD value of 0.59 Å. In the 4DW0 model, one of the methyl groups of the L340 side chain packs into the LN:A pocket of the downstream M2 helix, while the other one points into the pore, thereby blocking the ion conduction pathway (Fig. 3). Side-chain relaxation results in a shift of the L340 packing site from the LN:A site (PD = 2.1 Å) to the N:AG pocket (*PD* = 2.6 Å) due to rotation around the Cα—Cβ bond. This shift removes the block by methyl groups (Fig. 3). The A344 packing also undergoes changes after the side-chain relaxation. The 4DW0 A344 is in contact with L340 and G343 (*PD* = 2.3 Å) of the upstream M2 helix. After the restrained MD run, A344 packs into the L:GA pocket (*PD* = 2.5 Å), leading to a relatively more closed pathway at the A344 level. The packing of A347 undergo relatively small changes. The A347 side-chain packs in the G:LA pocket (*PD* = 2.3 Å) in 4DW0, and shift to a small ridge formed by G343 and A347 (denoted as GA·LA, *PD* = 2.4 Å). Removal of position restraints results in significant structural asymmetry (Fig. 4), as evident by the asymmetric packing patterns and shapes of the gating triangles. For example, the L340 side-chains packs into three different sites after 60-ns MD run: the LN:A, AG:L, and N:AG:L pockets. The packing patterns of A344 and A347 are also asymmetric (Fig. 4), and the tight packing of A344 at the C/B interface is lost. The 4DW0 TMD was also inserted into the POPC and SOPC bilayers, but the model was less stable, possibly due to the hydrophobic mismatch between the protein and the bilayers [7,26].

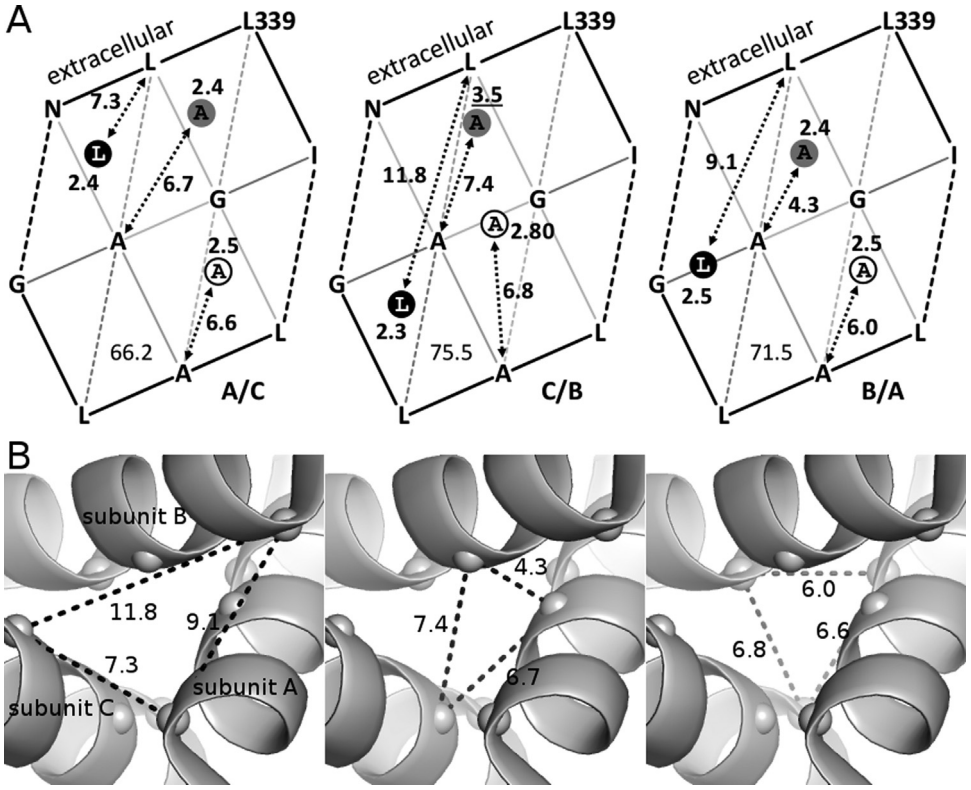

Fig. 4. Correlation between the packing patterns of L340, A344 and A447 and the P2X pore geometry in the MD-relaxed 4DW0 TMD. (A) Grid representations of residue packing between M2 helices at interfaces A/C (left), C/B (middle) and B/A (right). According to the contact criterion, the A344 packing at the C/B interface is lost. (B) The L340 (left), A344 (middle) and A347 (right) gating triangles.

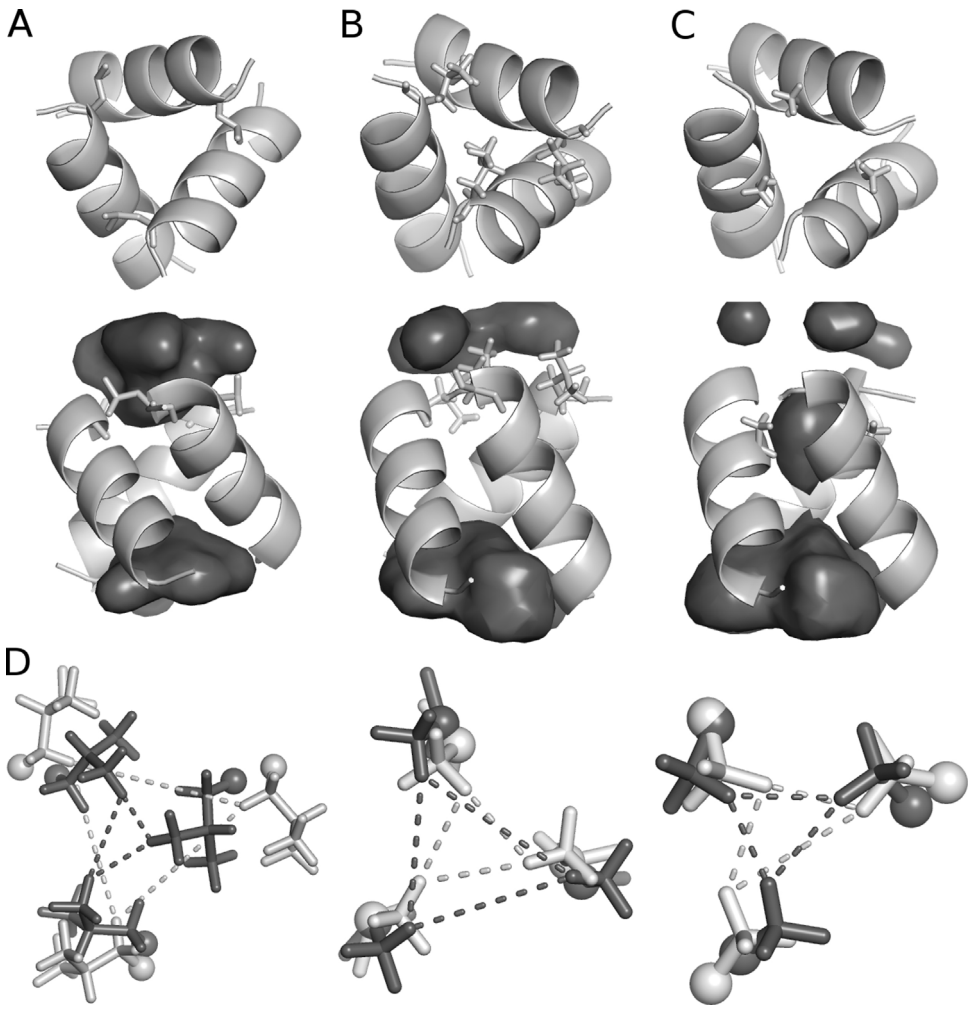

Fig. 5. Side-chain gating of the P2X TMD. (A–C) are cartoon representations of the gating blocks of P0-qTMD in the DLPC bilayer, P0-qTMD in the SOPC bilayer and A0-qTMD in the POPC bilayer, respectively. The top images in (A), (B) and (C) are viewed from the extracellular side. The bottom images are side-views of the gating blocks with surface representations of the solvent-accessible areas determined by the program HOLLOW. (D) Comparison of the side-chain configurations of L340 (left), A344 (middle) and A347 (right) between A0-qTMD relaxed in DLPC (light grey) and A0-qTMD relaxed in SOPC (dark grey). The Cα atoms of L340, A344 and A347 are represented by spheres and the side-chains are represented by sticks.

The P0-qTMD and A0-qTMD models deviate from 4DW0 by Cα-RMSDs of 3.35 and 3.23 Å, respectively. Both models were relaxed in DLPC, POPC and SOPC bilayers (Figs. S1 and S2). As expected, the average M2 tilt angles are decreased as the bilayer thickness increases, being 46.8° in DLPC ($n = 9$), 39.5° in POPC ($n = 9$) and 36.8° ($n = 9$) in SOPC bilayers. The average M2 crossing angles are also decreased as the bilayer thickness increases, being 77.8° in DLPC ($n = 9$), 66.5° in POPC ($n = 9$) and 62.2° in SOPC ($n = 9$). These data suggest that hydrophobic matching is the driving force behind changes in the tilt and crossing angles of M2 helices [1,20,2].

3.3. Geometric rules of channel gating by L340, A344 and A347

The MD simulations of 4DW0-TMD, P0-qTMD and A0-qTMD suggest simple rules for the regulation of pore size. First, the channel pore can be gated by the L340 side-chain reorientation, as demonstrated by the 4DW0 example (Fig. 3), in which the LN:A to N:AG shift removes pore block by methyl groups. This is also true of the TMD models relaxed by unrestrained MD simulation, as demonstrated by snapshots of the P0-qTMD (Fig. 5A) and the A0-qTMD (Fig. 5D) relaxed in DLPC. It seems that the opening of the L340 gate requires the removal of all three side-chain blocks (Fig. 5B and C). Despite the large size of hydrophobic side chain of leucine, only a small subset of side-chain orientations is frequently observed for the L340 knob. In one orientation in the LN:A pocket, the Cβ hydrogen atoms of the L340 knob point more toward the extracellular side, as seen in the 4DW0 model (Fig. 6A). In the MD-relaxed P2X-qTMD models, the Cβ hydrogen atoms point either more toward the extracellular side as in the 4DW0 model, or more toward the pore (Fig. 6B). These two orientations flip quickly in less than 40 ps (see Supplementary movie 3). The L340 side-chain orientations in the open configuration, based on the current MD data, are similar to the one seen in the 4DW0 model (Fig. 6C).

The orientation of the A344 side-chain is also important in regulation of the pore size (Fig. 5C and D). Compared to the L:GA site, the LL:G site is located further away from the pore axis, as demonstrated by a snapshot of A0-qTMD relaxed in the SOPC bilayer (Fig. 7), and the LL:G to L:GA shift orientates the side-chain more toward the pore lumen (Fig. 3; Fig. 5D), thus reducing the pore size. The orientations of A347 side-chains seems to be less consistently affected (Fig. 5D)

Second, the channel pore expands or constricts when the packing patterns of L340, A344 and A347 change, given that the gating segments do not undergo significant helical distortion. For L340, when the packing site shifts toward the C-terminus, namely, form the LN:A pocket to the N:AG:L region, the DCα(L340) is increased.

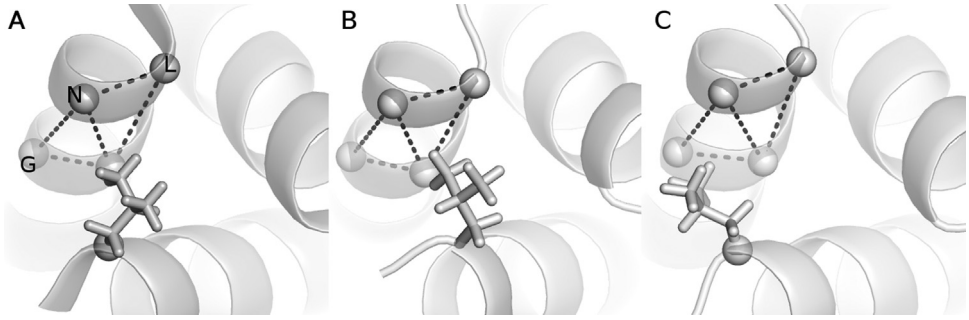

Fig. 6. L340 Side-chain orientations. (A) The 4DW0 L340 side-chain in blocking position, with the Cβ hydrogen atoms pointing more toward the extracellular side. (B) The L340 side-chain of A0-qTMD in blocking position, with the Cβ hydrogen atoms pointing more toward the pore. The structure is relaxed in SOPC lipids. (C) The L340 side-chain orientations after side-chain relaxation by restraint MD simulation.

The average DCα(L340) for the LN:A, N:AG, and N:AG:L pockets are 7.27 Å (n = 11), 9.05 Å (n = 8) and 9.66 Å (n = 7), respectively. In one case, the L340 side-chain is in close contact with N341 and G343 with the interface DCα(L340) being 6.50 Å. For A344, when the packing site moves toward the *N*-terminus, namely from the L:GA to the LL:G pockets (Fig. 7), the DCα(A344) is increased. The average DCα(A344) are 5.84 Å (n = 8) and 5.01 Å (n = 14) for the LL:G and L:GA pockets, respectively. In one case, A344 packs on the ridge formed by L340 and G343 (denoted as LL:GA), with DCα(A344) being 5.60 Å, possibly representing a transition state between the LL:G and L:GA packing configurations. In four cases, A344 packs on the ridge of L340 and A344 (LN·GA), with DCα(A344) being 5.12 Å. The variations of DCα (A347) is relatively small, with DCα(A347) values being 6.0 Å (n = 19) for G:LA, 6.4 Å (n = 2) for GA·LA and 6.0 (n = 6) for GA:A.

Third, changes in the packing patterns of L340, A344 and A347 are associated with changes in M2 tilts, which in turn alter the crossing angles between M2 helices around a packing unit located midway between the bilayer leaflets. This unit is formed by residue G343 and its packing pocket formed by A344, A347 and L348 (denoted as A:AL; PD = 2.51 Å, n = 27). This unit acts as a joint that allows helix rotation and displacement (Fig. 8). This is supported by the observation that at all M2 interfaces in different lipid bilayers, the upstream G343 (n = 27) is at the helix crossing points, and the downstream A344 (n = 22), A347 (n = 2) and A348 (n = 3) are at the helix crossing points. An early study also finds that glycine residues occur predominantly at helix crossing points between closely associated helices [10]. The packing patterns of L340 are most affected by changes in M2 tilts due to the fact that it is further away from the joint. Since the N:AG:L region is closer to the intracellular side than the LN:A pocket, shift of L340 side-chain away from the LN:A pocket requires tilting of either or both M2 helices at the interface in order for the L340 side-chain to reach the N:AG:L region (Fig. 6). The residues A344 and A347 are joint-forming residues and are on the extracellular and intracellular sides relative to the G343 knob, respectively. This implies that the packing patterns of A344 and A347 are less affected by changes in the M2 crossing angles alone. Data collected from the MD simulations show that the LL:G to L:GA shift also involves relative displacement of the M2 helices as indicated by the changes in the positions of the G343Cα atoms relative to the A:AL Cα atoms in a way that the G343 knob becomes closer to L348 residue when the M2 helices become more tilted (Fig. 8). This displacement avoids clashes between the downstream A347 and upstream L346 side-chains which could be caused by increase in the M2 crossing angles alone. This displacement favors the shift of A344 from LL:G to L:GA, but opposes the effect of M2 tilting on the A347 packing.

Fourth, the pore expansions at the L340 and A344 levels are mutually exclusive since M2 tilting that favors the expansion of the L340 gate opposes the expansion of the A344 gate. This mutual exclusion suggests that P2X gating involves sequential pore opening at L340 and A344 levels to allow ion conduction. This proposal is consistent with two seemingly different observations. In one study, the P2X2 gating residues have been placed in a region between I332 and I341, equivalent to the zfP2X4.1 L340 and L349, respectively [18]. More recently, the region is narrowed down to a segment from T336 and T339 [16], equivalent to zfP2X4.1 A344 and A347, respectively. It is possible that channel block by L340 is transient, while block by A344 and possibly by A347 represents desensitization states and requires longer time to recover. The

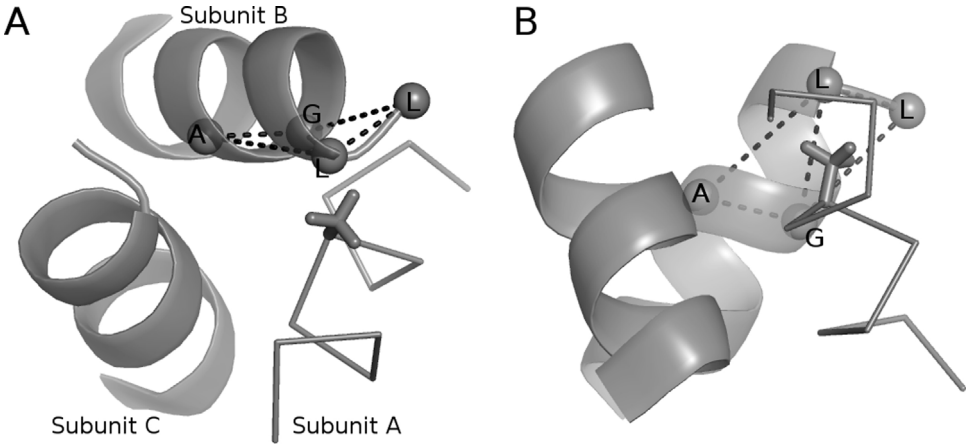

Fig. 7. Positions of the L:GA and LL:G pockets relative to the pore axis and the A344 knob. (A) is viewed from the extracellular side. (B) is the side view of the same structure. One M2 helix (subunit A) is shown as a ribbon, with the A344 knob shown as sticks. The LL:GA Cα-atoms of subunit B are shown as spheres.

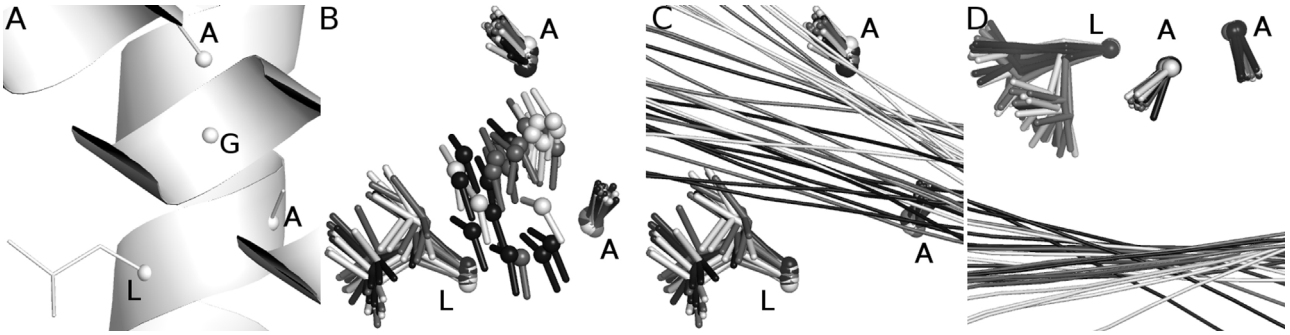

Fig. 8. G343 packing in the A:AL pocket. (A) Cartoon representation of a snapshot of P0-qTMD relaxed in POPC showing G343 packing in the A:AL pocket. The G343Cα-atom of is shown as a sphere, while the pocket forming residues A:AL are shown as sticks. Hydrogen atoms are not shown. (B) Views of the G343 packing units from P0-qTMD and A0-qTMD relaxed in SOPC (in light grey), POPC (in dark grey) and DLPC (in black). The A:AL Cα-atoms are aligned and shown as sticks. The G343Cα hydrogen atoms are shown as sticks. (C) The same G343 packing units as in (B), but the G343 knob residues are not shown. Instead, the axes of the upstream M2 helices are shown to indicate the crossing angles. (D) The G343 packing units viewed from the N-terminus of the downstream M2 helices, showing the rotations of the upstream M2 helices.

current picture of P2X gating differs from a previous one [19] in which expansion of the external pore and constriction of the internal pore are accomplished by reorienting the TM2 helices more towards the normal of the bilayer.

3.4. Transition of packing states

The geometric rules of P2X gating are inferred from snapshots of the P2X-qTMD models relaxed in different lipid bilayers by first restrained and then unrestrained MD simulations. To see the dynamic nature of residue packing, the A0-qTMD relaxed in SOPC is inserted into a DLPC bilayer, which is relaxed to match the hydrophobic length of the protein by a 5-ns MD run with position-restraints on all protein heavy atoms (i.e., non-hydrogen). Once the restraints are released, the A0-qTMD undergoes conformational adjustment to the DLPC bilayer, and the L340 packing sites shift toward the intracellular side. For example (Supplementary movie 1), the L340 knob at interface 1 shifts from the LN:A toward the N:AG pockets in about 150 ps, and remains in the N:AG pocket for about 500 ps until the downstream L348 joins to form the N:AG:L pocket. The L340 knob then remains in the N:AG:L pocket until the end of the MD run (30-ns) in DLPC. The replacement of SOPC with DLPC also induces changes in the packing patterns of A344 knobs. For example (Supplementary movie 2), the A344 knob at interface 1 transits from the ridge of L340 and G343 to the L:GA pocket in about 210 ps, and remains in the L:GA pocket until the end of the MD run.

The dynamics of residue packing was also examined for the A0-qTMD in a stable lipid environment. The unrestrained MD run of A0-qTMD in SOPC was extended for 10 ns. During this extended run, the L340 knob at interface 1 stays in the LN:A pocket (Supplementary movie 3), while the L340 knobs at interface 2 and 3 were found to jump between the LN:A and N:AG sites (Supplementary movie 3). The transitions are fast (from 30 to 200 ps), and can be consider instantaneous relative to the microsecond time scales resolved by single-channel recordings [22]. The fast transition rates are consistent with the observation that the transition pathways only involve small residue side chains (glycine and alanine) and the Cβ hydrogen atoms of asparagine or leucine (Supplementary movies 1 and 2), which may produce small energy barriers between packing states and underlie the fast and discrete nature of channel gating. The current data, however, are insufficient for statistical quantification of how fast the transitions take place, and how long a knob residue dwells in a particular site.

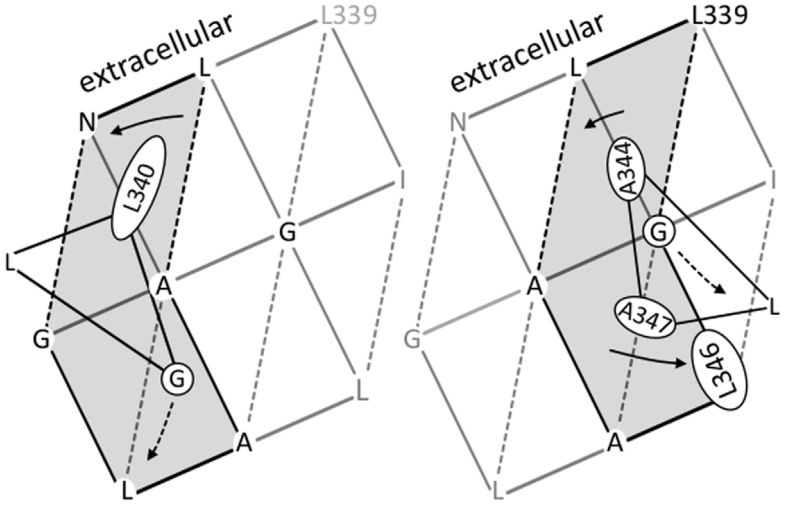

Fig. 9. Summary of the mechanisms of P2X channel gating. (A) L340 gating mechanism. The upstream L339, L340 and G343 and the downstream gating segment are shown as two-dimensional grids. The solid arrow indicates rotation around the glycine joint, and the dashed arrow indicates the G343 translation relative to the A:AL socket. The rotation and the translation are cooperate in L340 gating. (B) A344 and A347 gating mechanism. The upstream gating segment and the downstream A:AL socket are shown. A344 and A347 are in close proximity to each other and changes in their packing patterns are coupled. The solid arrows indicate rotation around the G343 joint, and the dashed arrow indicates the translation of G343 relative to the A:AL socket.

4. Conclusion

Despite different outcomes of MD simulations using different starting structures, a picture emerges of the P2X gating in which the packing patterns of L340, A344 and A347 determine the pore configurations (Fig. 9). The current MD study, however, is carried out in the absence of the extracellular domain (ECD) and simply provides a detailed description of the gating sections of the M2 helix. It is known that the ECD plays important roles not only in channel gating, but also in cation permeation through the transmembrane pathway [24]. The ECD has a central vestibule of a negative electrostatic surface potential [13,14], and may increase the local cation concentrations near the extracellular mouth of the transmembrane pathway and thus facilitate transmembrane ion flows. More work is needed to incorporate the ECD for a full length P2X receptor model in order to clarify the issues of ion permeation and the physical rules of channel gating. It is especially interesting to see how the ECD–TMD coupling modifies the spontaneous changes in the packing patterns relevant to channel gating.

Appendix A. Supplementary data

Supplementary data associated with this article can be found, in the online version, at http://dx.doi.org/10.1016/j.jmgm.2015.06.015

References

[1] O.S. Andersen, R.E. Koeppe 2nd, Bilayer thickness and membrane protein function: an energetic perspective, Annu. Rev. Biophys. Biomol. Struct. 36 (2007) 107–130.
[2] A. Benjamini, B. Smit, Robust driving forces for transmembrane helix packing, Biophys. J. 103 (6) (2012) 1227–1235.
[3] R.B. Best, X. Zhu, J. Shim, P.E. Lopes, J. Mittal, M. Feig, A.D. Mackerell Jr., Optimization of the additive CHARMM all-atom protein force field targeting improved sampling of the backbone φ, ψ and side-chain χ_1 and χ_2 dihedral angles, J. Chem. Theory Comput. 8 (9) (2012) 3257–3273.
[4] T. Darden, D. York, L. Pedersen, Particle mesh Ewald: a N-log(n) method for Ewald sums in large systems, J. Chem. Phys. 98 (12) (1993) 10089–10092.
[5] M. Hattori, E. Gouaux, Molecular mechanism of ATP binding and ion channel activation in P2X receptors, Nature 485 (7397) (2012) 207–212.
[6] B. Hess, H. Bekker, H.J.C. Berendsen, J.G.E.M. Fraaije, LINCS: a linear constraint solver for molecular simulations, J. Comp. Chem 18 (12) (1997) 1463–1472.
[7] G. Heymann, J. Dai, M. Li, S.D. Silberberg, H.X. Zhou, K.J. Swartz, Inter- and intrasubunit interactions between transmembrane helices in the open state of P2X receptor channels, Proc. Natl. Acad. Sci. U. S. A. 110 (2013) E4045–E4054.
[8] B.K. Ho, F. Gruswitz, HOLLOW: generating accurate representations of channel and interior surfaces in molecular structures, BMC Struct. Biol. 8 (2008) 49.
[9] J.P. Jämbeck, A.P. Lyubartsev, Derivation and systematic validation of a refined all-atom force field for phosphatidylcholine lipids, J. Phys. Chem. B 116 (10) (2012) 3164–3179.
[10] M.M. Javadpour, M. Eilers, M. Groesbeek, S.O. Smith, Helix packing in polytopic membrane proteins: role of glycine in transmembrane helix association, Biophys. J. 77 (3) (1999) 1609–1618.
[11] H. Joo, A.G. Chavan, J. Phan, R. Day, J. Tsai, An amino acid packing code for α-helical structure and protein design, J. Mol. Biol. 419 (3–4) (2012) 234–254.
[12] W.L. Jorgensen, J. Chandrasekhar, J.D. Madura, R.W. Impey, M.L. Klein, Comparison of simple potential functions for simulating liquid water, J. Chem. Phys. 79 (2) (1983) 926–935.
[13] T. Kawate, J.C. Michel, W.T. Birdsong, E. Gouaux, Crystal structure of the ATP-gated $P2X_4$ ion channel in the closed state, Nature 460 (7255) (2009) 592–598.
[14] T. Kawate, J.L. Robertson, M. Li, S.D. Silberberg, K.J. Swartz, Ion access pathway to the transmembrane pore in P2X receptor channels, J. Gen. Physiol. 137 (6) (2011) 579–590.
[15] J.B. Klauda, R.M. Venable, J.A. Freites, J.W. O'Connor, D.J. Tobias, C. Mondragon-Ramirez, I. Vorobyov, A.D. MacKerell Jr., R.W. Pastor, Update of the CHARMM all-atom additive force field for lipids: validation on six lipid types, J. Phys. Chem. B 114 (23) (2010) 7830–7843.
[16] S. Kracun, V. Chaptal, J. Abramson, B.S. Khakh, Gated access to the pore of a P2X receptor: structural implications for closed-open transitions, J. Biol. Chem. 285 (13) (2010) 10110–10121.
[17] N. Kučerka, M.P. Nieh, J. Katsaras, Fluid phase lipid areas and bilayer thicknesses of commonly used phosphatidylcholines as a function of temperature, Biochim. Biophys. Acta 1808 (11) (2011) 2761–2771.
[18] M. Li, T.H. Chang, S.D. Silberberg, K.J. Swartz, Gating the pore of P2X receptor channels, Nat. Neurosci. 11 (8) (2008) 883–887.
[19] M. Li, T. Kawate, S.D. Silberberg, K.J. Swartz, Pore-opening mechanism in trimeric P2X receptor channels, Nat. Commun. 1 (2010) 44.
[20] C. Muhle-Goll, S. Hoffmann, S. Afonin, S.L. Grage, A.A. Polyansky, D. Windisch, M. Zeitler, J. Bürck, A.S. Ulrich, Hydrophobic matching controls the tilt and stability of the dimeric platelet-derived growth factor receptor (PDGFR) β transmembrane segment, J. Biol. Chem. 287 (31) (2012) 26178–26186.
[21] J.-L. Popot, D.M. Engelman, Membrane protein folding and oligomerization: the two-stage model, Biochemistry 29 (17) (1990) 4031–4037.
[22] J.K. Rosenstein, S. Ramakrishnan, J. Roseman, K.L. Shepard, Single ion channel recordings with CMOS-anchored lipid membranes, Nano Lett. 13 (6) (2013) 2682–2686.
[23] A. Sali, T.L. Blundell, Comparative modelling by satisfaction of spatial restraints, J. Mol. Biol. 234 (3) (1993) 779–815.
[24] D.S. Samways, Z. Li, T.M. Egan, Principles and properties of ion flow in P2X receptors, Front. Cell. Neurosci. 8 (2014), 6.
[25] M.G. Wolf, M. Hoefling, C. Aponte-Santamaría, H. Grubmüller, G. Groenhof, g_membed: efficient insertion of a membrane protein into an equilibrated lipid bilayer with minimal perturbation, J. Comput. Chem. 31 (11) (2010) 2169–2174.
[26] H.X. Zhou, T.A. Cross, Influences of membrane mimetic environments on membrane protein structures, Annu. Rev. Biophys. 42 (2013) 361–392.